
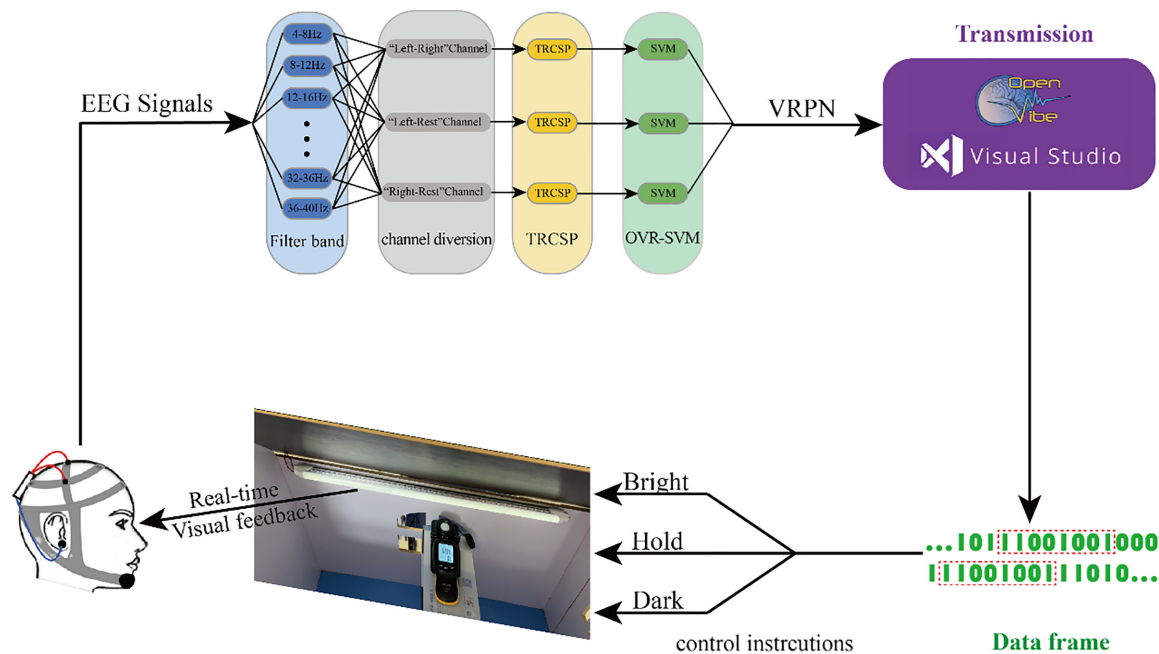


# MI-based BCI with accurate real-time three-class classification processing and light control application

*Proc IMechE Part H:*  
*J Engineering in Medicine*  
 2023, Vol. 237(8) 1017–1028  
 © IMechE 2023  
 Article reuse guidelines:  
[sagepub.com/journals-permissions](https://sagepub.com/journals-permissions)  
 DOI: 10.1177/09544119231187287  
[journals.sagepub.com/home/pih](https://journals.sagepub.com/home/pih)  


Jiakai Zhang<sup>1</sup>, Boyang Xu<sup>1</sup>, Xiongjie Lou<sup>1</sup>, Yan Wu<sup>1</sup>  
 and Xiaoyan Shen<sup>1,2</sup>

## Graphical abstract



## Abstract

The use of brain–computer interfaces (BCIs) to control intelligent devices is a current and future research direction. However, the challenges of low accuracy of real-time recognition and the need for multiple electroencephalographic channels are yet to be overcome. While a number of research teams have proposed many ways to improve offline classification accuracy, the potential problems in real-time experiments are often overlooked. In this study, we proposed a label-based channel diversion preprocessing to solve the problem of low real-time classification accuracy. The Tikhonov regularised common spatial-pattern algorithm (TRCSP) and one vs rest support vector machine (OVR-SVM) were used for feature extraction and pattern classification. High accuracy was achieved in real-time three-class classification using only three channels (average real-time accuracy of 87.46%, with a maximum of 90.33%). In addition, the stability and reliability of the system were verified through lighting control experiments in a real environment. Using the autonomy of MI and real-time feedback of light brightness, we have built a fully autonomous interactive system. The improvement in the real-time classification accuracy in this study is of great significance to the industrialisation of BCI.

<sup>1</sup>School of Information Science and Technology, Nantong University, Nantong, China

<sup>2</sup>Nantong Research Institute for Advanced Communication Technologies, Nantong University, Nantong, China

## Corresponding author:

Xiaoyan Shen, School of Information Science and Technology, Nantong University, Nantong, Jiangsu Province 226019, China.

Email: [xiaoyansho@ntu.edu.cn](mailto:xiaoyansho@ntu.edu.cn)

## Keywords

Brain–computer interface, motor imagery, channel diversion preprocessing, three-class classification, real-time control

Date received: 13 April 2023; accepted: 23 June 2023

## Introduction

With the rapid development of computer science and neuroscience technology, brain–computer interfaces (BCIs) have enabled direct communication between the human brain and external devices.<sup>1,2</sup> The BCI is a novel intelligent interaction technology that can be used to read brain activity directly and apply it to real-time control. Currently, the BCI technology has been applied in many areas. For instance, Xiong et al.<sup>3</sup> and Yu et al.<sup>4</sup> developed wheelchair control systems based on motor-imagery (MI) electroencephalography (EEG) signals. Further, Xu et al.<sup>5</sup> achieved three-dimensional control of a robotic arm using a non-invasive EEG record device and an eye-movement tracker. Borgheai et al.<sup>6</sup> developed a BCI communication system based on functional near-infrared spectroscopy, and Peters et al.<sup>7</sup> presented a shuffle speller typing interface based on a modified eye-tracker and Steady State Visual Evoked Potential. Although these control schemes can serve as a reference, they are plagued by certain shortcomings. The control method using SSVEP or P300 cannot be separated from the display, which considerably affects portability. Moreover, the high-frequency flicker of such types of paradigms can also result in visual fatigue among users. To improve the accuracy, 32-ch or 64-ch EEG caps are commonly used; however, this increases the cost and reduces wearing comfort.<sup>8</sup>

In addition, to achieve control over external intelligent devices, the accuracy of real-time classification results considerably affects the control results. Abenna et al.<sup>9</sup> combined the light gradient boosting machine classifier and the sine cosine algorithm to select the optimal channel and establish the better prediction models, which remarkably improved the accuracy of the binary classification. Jeyabalan et al.<sup>10</sup> combined adaptive band pass filters and adaptive autoregressive for classification of left and right MI signals. This combination effectively enhanced the EEG signal and reduced noise. Qiu et al.<sup>11</sup> preprocessed the raw evoked potential (EP) with Gaussian radial basis function neural network, which was then input it into an adaptive signal enhancer. Consequently, the system could efficiently track changes in the EP to achieve higher classification accuracy. Iacoviello et al.<sup>12</sup> proposed a two stage algorithm for real-time EEG processing. The first stage was used for feature determination and classifier training, and the second stage employed principal component analysis for signals to avoid signal redundancy. These research teams have made significant contributions in improving classification accuracy; however, the proposed algorithms

were only applied to real-time classification after obtaining good results in the offline experiment. Therefore, the signal conditions that may occur during real-time signal transmission were not considered.

This study used a label-based channel diversion preprocessing to divert real-time transmitted signals. Simultaneously, to achieve obstacle free control, reduce channel waste and improve user comfort, C3, C4 and Cz channels were selected to collect MI EEG signals. Further three classifications were implemented using filter bank Tikhonov regularised common spatial pattern (FB-TRCSP). To evaluate the accuracy and feasibility of the system in real environment, the proposed system was applied to real LED brightness control. The system required the subject to imagine ‘left’, ‘right’ and ‘rest’ to dim, brighten and hold LED brightness, respectively. From the perspective of LED control results, the system can provide a simple, convenient and highly accurate control scheme with three dimensions for intelligent device interaction. In subsequent research, more dimensional control systems can be created through the combination of different instructions.

## Methods

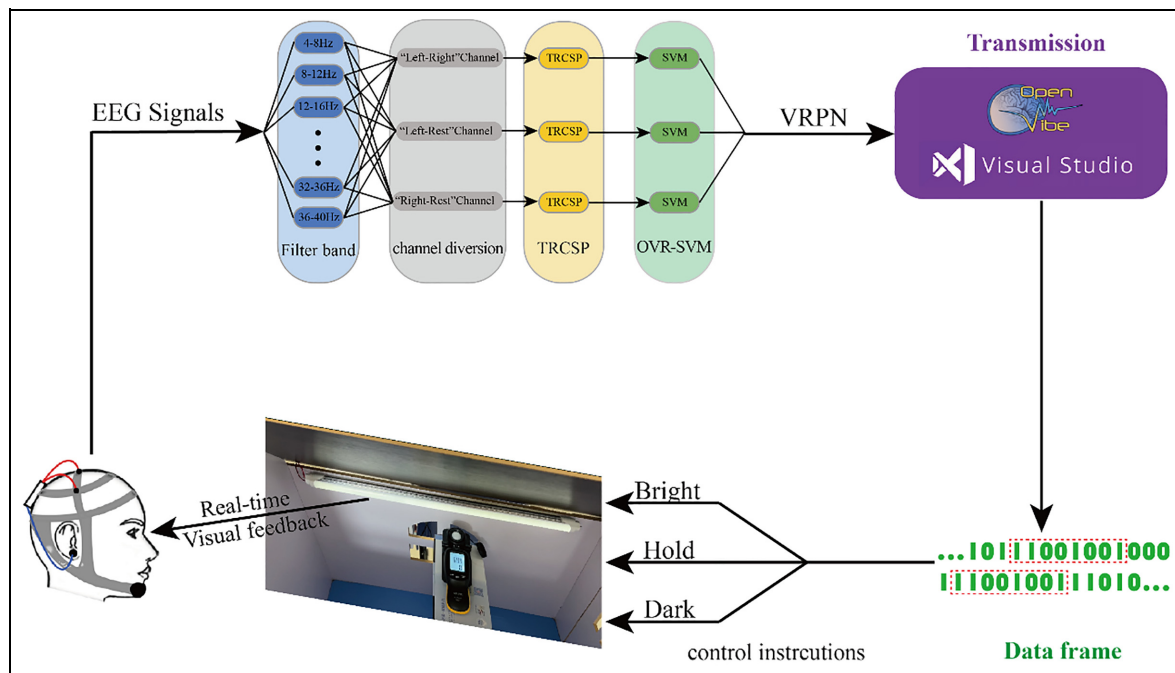
### System design

The architecture of the MI-based real-time control system designed is shown in Figure 1.

The system comprised an EEG signal acquisition module, a signal processing module and an LED brightness control module. Prior to the experiment, subjects were trained on various MI tasks (imagining left- and right-hand movements and rest). Following the completion of training, the system generated a customised decoder that was loaded into OpenViBE’s real-time processing module to start the real-time control experiment. The processed three-class classification results were converted into control commands. These were transmitted wirelessly to the pulse width modulation (PWM) control module for brightening, dimming and maintaining the brightness of the LEDs (imagine right corresponding to brightening, imagine left corresponding to dimming and rest to maintain brightness). In the real-time control session, the subjects can adjust the three signals according to the brightness of the light by themselves.

### EEG signal acquisition module

OpenBCI (OpenBCI, New York, NY, USA) with a sampling frequency of 250 Hz was used as the EEG



**Figure 1.** System process and architecture.

signal acquisition device. When subjects were instructed to perform MI tasks, the relevant areas of the cerebral cortex stimulated a response and subsequently generated regularly varying EEG signals. Consequently, the high stability and variability of the EEG signals that occurred at these specific times were considered as the physiological basis for the use of MI EEG signals as the input to the BCI system.<sup>13</sup> When unilateral limb movements were imagined, the  $\mu$  (8–12 Hz) and  $\beta$  (13–30 Hz) rhythms in the contralateral primary sensorimotor cortical areas of the brain exhibited a considerable decrease in energy. This is known as event-related desynchronisation (ERD). Conversely, the energy of rhythms in the ipsilateral primary sensorimotor cortical areas increased considerably. This result is known as event-related synchronisation (ERS).<sup>14</sup> Because EEG signals associated with imagining left–right movements are typically concentrated around the C3 and C4 regions, only three electrodes, C3, Cz and C4, were used as the measurement electrodes to reduce the difficulty of multichannel data processing and improve the wearing comfort of users. These electrodes were placed according to the 10–20 international standard system.<sup>15</sup>

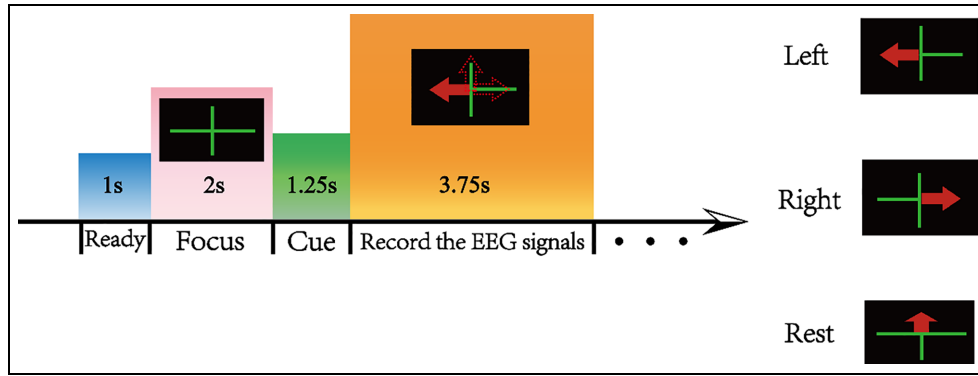
Nine participants, including seven men and two women, with a mean age of  $24 \pm 0.67$  years were recruited for the experiment. Each participant was first given sufficient time to familiarise themselves with the EEG cap and the experimental acquisition process. This process required 10–15 min. Subsequently, the formal training session of the experiment was conducted. During the training session, each participant was asked to perform 10 groups of experiments, and each experiment comprised three left–right MI and rest tasks each.

OpenViBE (<http://openvibe.inria.fr>) is a free and open-source software. OpenBCI and OpenViBE's 'Acquisition Server' were connected to obtain real-time, high-resolution signals of brain activity.<sup>16</sup> Thereafter, the MI BCI stimulator was opened to provide stimulus cues to the subjects. The stimulus cues were categorised into left, right and up arrows, with the left and right arrows representing imagine left and right movements, respectively, and the up arrow indicating rest. All three arrows appeared randomly and at the same interval. Subjects performed the corresponding MI task according to the stimulus cues, and the computer recorded the brain activity state. The experimental paradigm is shown in Figure 2.

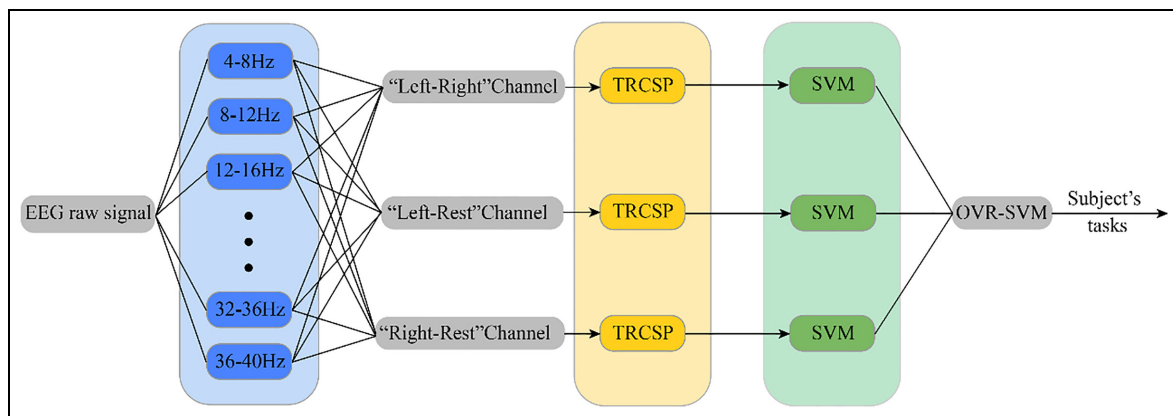
### EEG decoder based on the channel selection FB-TRCSP algorithm with one-vs-rest SVM

Although the common spatial pattern (CSP) algorithm is widely used for feature extraction in MI tasks, the problems of multichannel analysis requirement, susceptibility to noise, and overfitting render the classification less effective.<sup>17–19</sup> Considering that this study was oriented towards real-time control applications, the FB-TRCSP algorithm was used to optimise the problems and improve the accuracy of real-time classification. The proposed learning method is shown in Figure 3.

**Filter bank.** Because the operating band of the EEG signal directly affects the performance of the spatial filter, setting the appropriate frequency range is highly desired. In this study, the 4–40 Hz band was divided



**Figure 2.** Three-class MI process and paradigm.



**Figure 3.** Proposed FB-TRCSP learning approach with OVR-SVM.

using nine filters: 4–8, 8–12, 12–16, 16–20, 20–24, 24–28, 28–32, 32–36 and 36–40 Hz. In subsequent filtering, the signal in the band can be filtered according to its quality, and band-specific filter characteristics can be generated.<sup>20</sup>

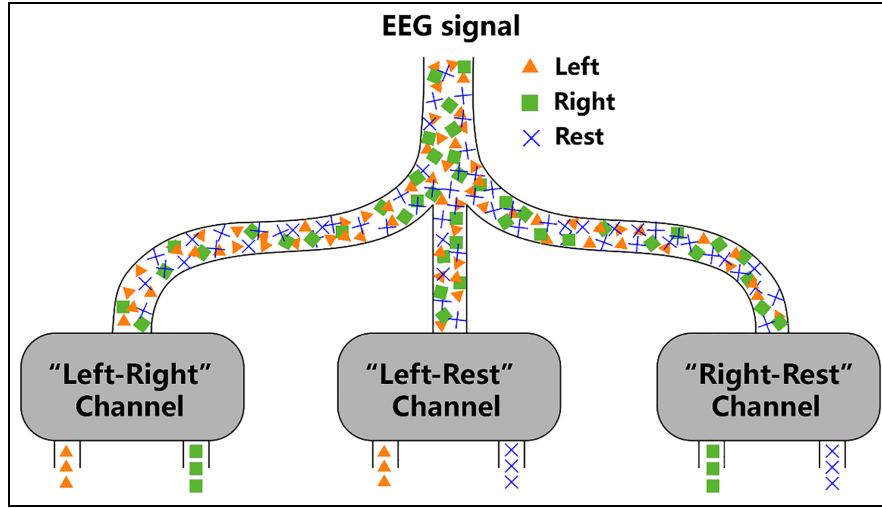
**Label-based three-class channel diversion preprocessing.** The basic principle of real-time processing is that through offline training, three types of EEG signal characteristics of the subject can be obtained. After inputting the characteristics as real-time discrimination criteria into the receiving module, the system matches the EEG signals received in real time and outputs discrimination results.<sup>9</sup> However, in real-time classification experiments, it is not guaranteed that subjects will always emit the same target EEG signal in a single task; thus, nontarget signals can be considered interference signals that seriously affect the accuracy of real-time classification. To solve the problem of low accuracy in real-time classification, we proposed a label-based channel diversion preprocessing. Each sampled signal will receive a corresponding channel label. Feature channels were divided into the ‘Left–Right’, the ‘Left–Rest’ and the ‘Right–Rest’ channels. The classification logic is shown in Figure 4.

The signals containing ‘left’, ‘right’ and ‘rest’ labels are input in all three channels simultaneously. When the label by the signal matched the channel label, the signal was allowed to pass through, otherwise the signal was rejected.

**TRCSP.** During MI, the ERS and ERD phenomena can cause changes in the power spectrum of the  $\mu$ - and  $\beta$ -rhythms in the EEG signal.<sup>9</sup> Therefore, feature extraction of such energy variations can be performed using spatial filters. The CSP algorithm uses the spatial distribution of the features to project the EEG signal into a subspace and the diagonalisation of the matrix to determine an optimal set of spatial filters for the projection that maximises the difference in variance values between the two types of signals, thus resulting in the most discriminating feature vector.<sup>21,22</sup> The objective function is expressed as follows:

$$J(\omega) = \frac{\omega^T X_1^T X_1 \omega}{\omega^T X_2^T X_2 \omega} = \frac{\omega^T C_1 \omega}{\omega^T C_2 \omega}, \quad (1)$$

where  $\omega$  is the spatial filter trained from the extracted feature vectors,  $T$  represents the transpose,  $X_i$  is the data matrix of the motion imagery classes and  $C_i$  is the



**Figure 4.** Logic of label-based three-class channel selection.

covariance matrix of classes 1 and 2. Although the CSP algorithm can gain algorithmic advantages in time and space, there is an overfitting problem when the data sample is excessively small.

To overcome the overfitting problem, the Tikhonov regularised CSP (TRCSP) algorithm was used in this study. The regularisation of the CSP at the level of the objective function (equation (1)) is obtained by imposing a prior on the spatial filter to penalise solutions that do not satisfy the prior information. In equation (2),  $P(\omega)$  is the penalty function used to measure the degree to which the spatial filter  $\omega$  satisfies the given prior condition. The more conditions that  $\omega$  satisfies, the smaller the value of  $P(\omega)$ . The TRCSP algorithm combines CSP with Tikhonov regularisation (TR). TR is a classical regularisation model, which was first introduced into regression problems to handle penalty terms using weights. The penalty term  $P(\omega)$  for the TRCSP algorithm is expressed as follows:

$$J(\omega) = \frac{\omega^T C_1 \omega}{\omega^T C_2 \omega + \alpha P(\omega)}, \quad (2)$$

$$P(\omega) = \omega^2 = \omega^T \omega = \omega^T I \omega, \quad (3)$$

where  $I$  is the identity matrix. The regularisation parameter  $\alpha$  in equation (2) is the Tikhonov coefficient. A larger  $\alpha$  implies a higher TR. With limited training data, or noise, the optimisation process of adjusting  $\alpha$  can result in an effective spatial filter. Following numerous adjustment attempts, the parameter  $\alpha$  was set to 3.

One advantage of TRCSP is that the new objective function is still a generalised eigenvalue problem, which can be solved via standard methods. However, the addition of the regularisation term eliminates the numerator–denominator symmetry in the objective function. Therefore, the eigenvalues should be determined twice to obtain the final spatial filter.

Specifically, we must solve the following two objective functions:

$$J_1(\omega) = \frac{\omega^T C_1 \omega}{\omega^T C_2 \omega + \alpha \omega^T I \omega}, \quad (4)$$

$$J_2(\omega) = \frac{\omega^T C_2 \omega}{\omega^T C_1 \omega + \alpha \omega^T I \omega}. \quad (5)$$

Maximising  $J_1(\omega)$  renders the variance of the first task larger and that of the second task smaller, whereas maximising  $J_2(\omega)$  achieves the opposite. The eigenvector matrices obtained by solving the objective functions were as follows.

$$M_1 = (C_2 + \alpha I)^{-1} C_1 \quad (6)$$

$$M_2 = (C_1 + \alpha I)^{-1} C_2 \quad (7)$$

The eigenvector corresponding to the maximum eigenvalue was used to form the optimal spatial filter  $\omega$ . The subsequent feature extraction method was the same as that of traditional CSP.

**OVR-SVM.** The support vector machine (SVM)<sup>23</sup> is widely used for real-time EEG signal binary classification problems<sup>24</sup> because of its excellent real-time processing capability for large data and small arithmetic power requirement. We used three sets of SVM classifiers to implement the three-class classification of real-time EEG signals.

Three sets of OVR-SVM classifiers were ‘left vs right and rest’, ‘right vs left and rest’ and ‘rest vs left and right’. The principle involves using the target sample as the positive set and the remaining samples as the negative set. The ratio of training and testing sets was 7:3. Only the results of the positive set were obtained for each set of classifiers  $f_i(x)$ ,  $x = 1, 2, 3$ . Consequently,

the result files were combined into a single triple classification output. In real-time classification, the largest  $f_i(x)$  was used as the output.

### LED control

Three EEG signals and three control commands were used: 'imagine right' corresponds to brightening, 'imagine left' to dimming and 'rest' to a brightness hold.

**Data frame.** A data frame comprises three parts: the header, data and end of the frame. The header was used to identify the beginning of a data frame and the tail was used to indicate the end of a piece of data.

In this system, an eight-bit data frame format was used to send control commands. Here, 100 was assigned to the 'Dark' instruction, 001 to the 'Bright' instruction and 010 to the 'Hold' instruction. Of the remaining five bits, three bits were allocated to the head of the frame, and two bits were allocated to the tail. For accurate recognition by the receiver, the header and tail were set to 111 and 00, respectively.

When the receiver detects an incoming data frame with three consecutive 1s, this sequence is recognised as a frame header. The next five bits are automatically assigned to the detection range, the values of bits 4, 5 and 6 are extracted, and the corresponding operation is output. The frame tail is then discarded, and the next data frame is prepared for reception.

**Transmission through virtual reality peripheral network.** The conversion of classification results into control commands is a critical step in the realisation of real-time control of EEG signals. The virtual reality peripheral network (VRPN) was used for data transmission.<sup>25</sup> The VRPN comprises a series of libraries for data communication between the application and external devices, compiled mainly in Microsoft Visual Studio C++.<sup>26</sup>

According to the previous section, three feature channels were obtained in the three-class preprocessing session. Therefore, the VRPN outputs a three-channel probability. This flowchart is illustrated in Figure 5.

In the 'Left-Right' channel, a probability value greater than 0.5 denotes 'imagine right'. Consequently, the system will send '11100100' to the control board, and the light will become brighter, and vice versa. The 'Left-Rest' and 'Right-Rest' channels operate in a similar manner.

**PWM.** PWM is a series of pulses of equal amplitude output through the control of a circuit switching device. The voltage is applied to the load in a repetitive sequence of pulses with a connection of 1 or a disconnection of 0. The analogue voltage signal converted using digital signals was obtained by varying the duty cycle of the square wave.<sup>27</sup>

LEDs controlled by PWM waves do not stay ON all the time during illumination. Because the diodes switch ON and OFF rapidly, they can be switched ON and OFF once in a short period, and the human eye cannot detect flickers at frequencies greater than 200 Hz. Therefore, the LEDs remain ON all the time to the human eye. The PWM wave is used to control the percentage of time the LED is ON and OFF in one cycle, and by adjusting the pulse width of the PWM wave, the brightness of the LED can be controlled. The implementation principle is illustrated in Figure 6.

The counter in the development board counts from bottom to top. When the count value reaches the set value *COMP*, a high level is output, and the LED is switched ON. When the count value reaches the maximum count value *COUNTERTOP*, the counter is reset, a low level is output, and the LED is switched off. As the *COMP* value increases, the high-level duration becomes shorter, and the LED becomes dimmer. Accordingly, when the *COMP* value decreases, the high-level duration becomes longer and LED brightness increases. By setting each brightness level to a distinct *COMP* value, the brightness can be adjusted by changing the *COMP* value in the PWM programme to change the brightness of the LEDs.

## Experimental results

### Performance of the real-time three-class MI task

Table 1 presents the accuracy rates for each MI task for all nine participants as well as the average accuracy rate.

Table 1 reveals that the average recognition rate for the nine participants was greater than 87%, and the recognition accuracy for three subjects was more than 90%.

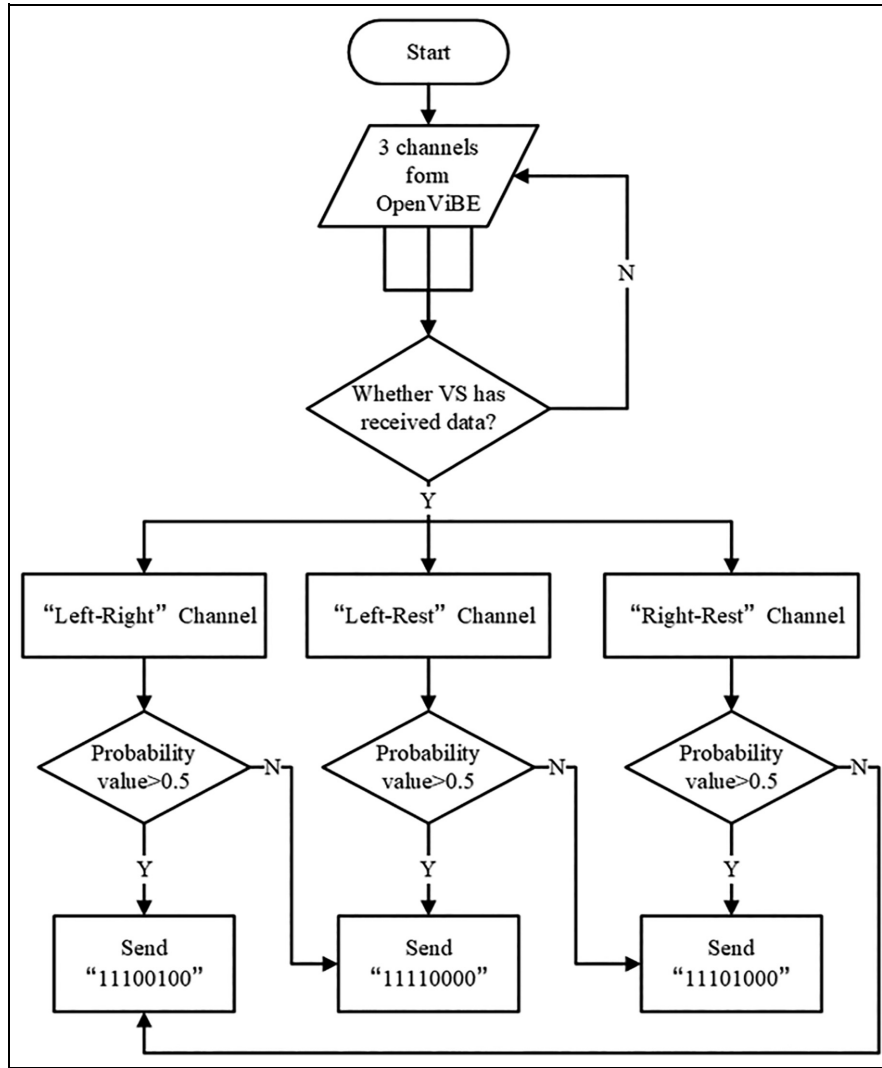
### Performance of LED control

To evaluate the accuracy and feasibility of the system in real environment, we applied the system to real LED brightness control. To verify the control effect and analyse the results of the experiment, three sets of experiments were designed: continuous brightening, continuous darkening and alternating brightness. The first two experiments lasted 20 s and the third experiment lasted 30 s. The minimum luminance level was 0 and the maximum was 100. To save time, the variation was set to five luminance levels per second.

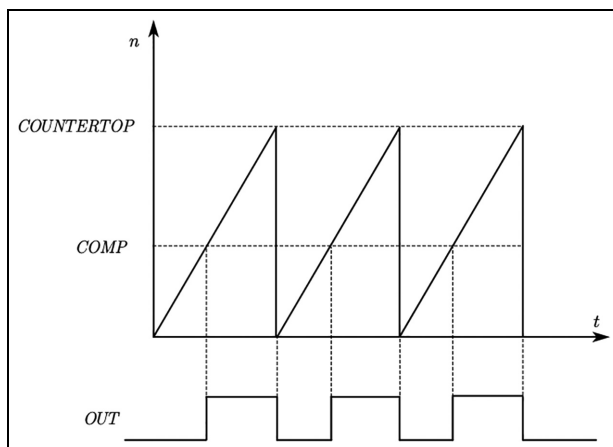
**Continuous brightening.** The luminance level was set to 0 before beginning the experiment and the participants were asked to imagine right-hand movement. The luminance effect was observed, and the change curve was recorded as shown in Figure 7.

Grey shading indicates the delay in the entry of the entry of participants into the state, the magenta dots indicate abnormal time points and the yellow section





**Figure 5.** Instruction transmitting process by VRPN.



**Figure 6.** The working principle of pulse width modulation.

$$Dev = \frac{\sum_{i=0}^N d_i}{N}, \quad (8)$$

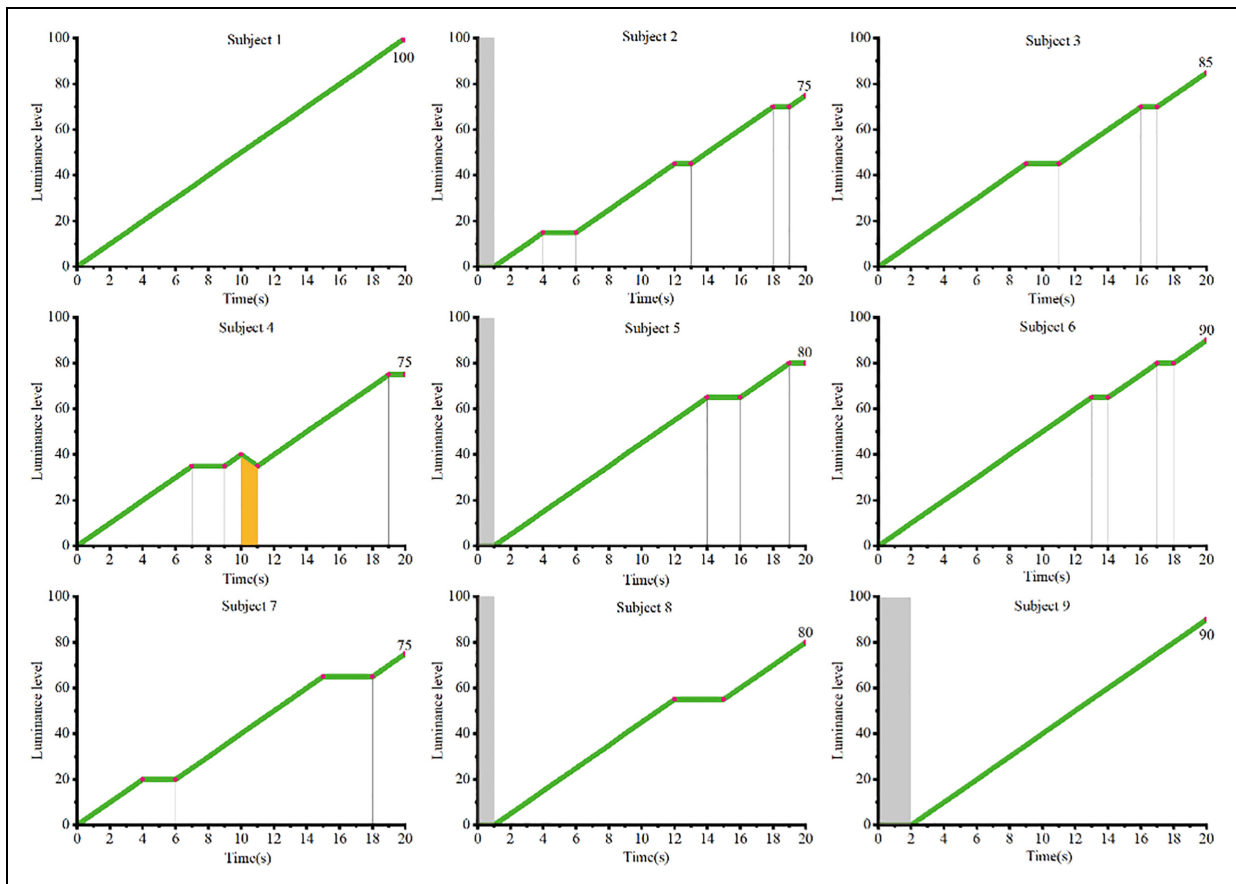
$$d_i = \frac{|Ax + B\hat{y} + C|}{\sqrt{A^2 + B^2}}, \quad (9)$$

where  $N$  is the number of time nodes in an experiment,  $\hat{y}$  is the vertical coordinate value of the bias and  $d_i$  is the difference in the distance between the offset and theoretical nodes. The offset value reflects the amount of deviation from the theoretical value produced by the subject at each time node of the real-time control. The  $Dev$  dotted line plots for the nine participants are shown in Figure 8.

indicates the period when the ‘Dark’ command occurred.

To quantify the control accuracy, the offset,  $Dev$ , is defined as follows:

**Continuous darkening.** The luminance level was set to 100 and the participants were asked to imagine left hand movement. The luminance effect was observed, and the change curve was recorded (Figure 9).



**Figure 7.** Results of nine participants in the continuous brightening experiment.

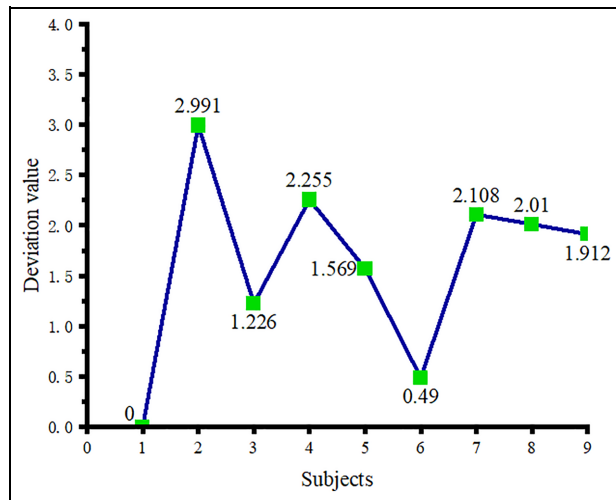
**Table 1.** Recognition accuracy for nine participants.

Subject	'Left' recognition accuracy (%)	'Right' recognition accuracy (%)	'Rest' recognition accuracy (%)	Total recognition accuracy (%)
1	85.88	100.00	85.10	90.33
2	94.05	86.60	89.92	90.19
3	85.11	90.77	88.52	88.13
4	90.20	88.10	79.85	86.05
5	95.70	90.11	81.22	89.01
6	86.01	97.88	76.99	86.96
7	78.93	92.51	83.96	85.13
8	90.63	91.16	78.40	86.73
9	87.21	94.70	88.27	90.06
10	88.09	89.11	83.82	87.01
11	89.01	87.53	82.05	86.20
12	85.49	88.33	90.56	88.13
13	92.81	95.11	82.68	90.20
14	86.39	87.61	79.94	84.65
15	84.98	89.41	85.62	86.67
16	79.76	88.23	83.84	83.94
Average accuracy	87.52 $\pm$ 4.57	91.07 $\pm$ 3.95	83.80 $\pm$ 4.06	87.46 $\pm$ 2.07

Grey shading indicates the delay in the entry of the participant into the state, the magenta dots indicate abnormal time points and the yellow section indicates

the time period when the 'Bright' command occurred. The *Dev* dotted line plots for the nine participants are shown in Figure 10.





**Figure 8.** Dev value of the continuous brightening experiment.

In the continuous darkening experiment, the number of subjects with delayed entry increased, and the deviation from the descent curve was greater.

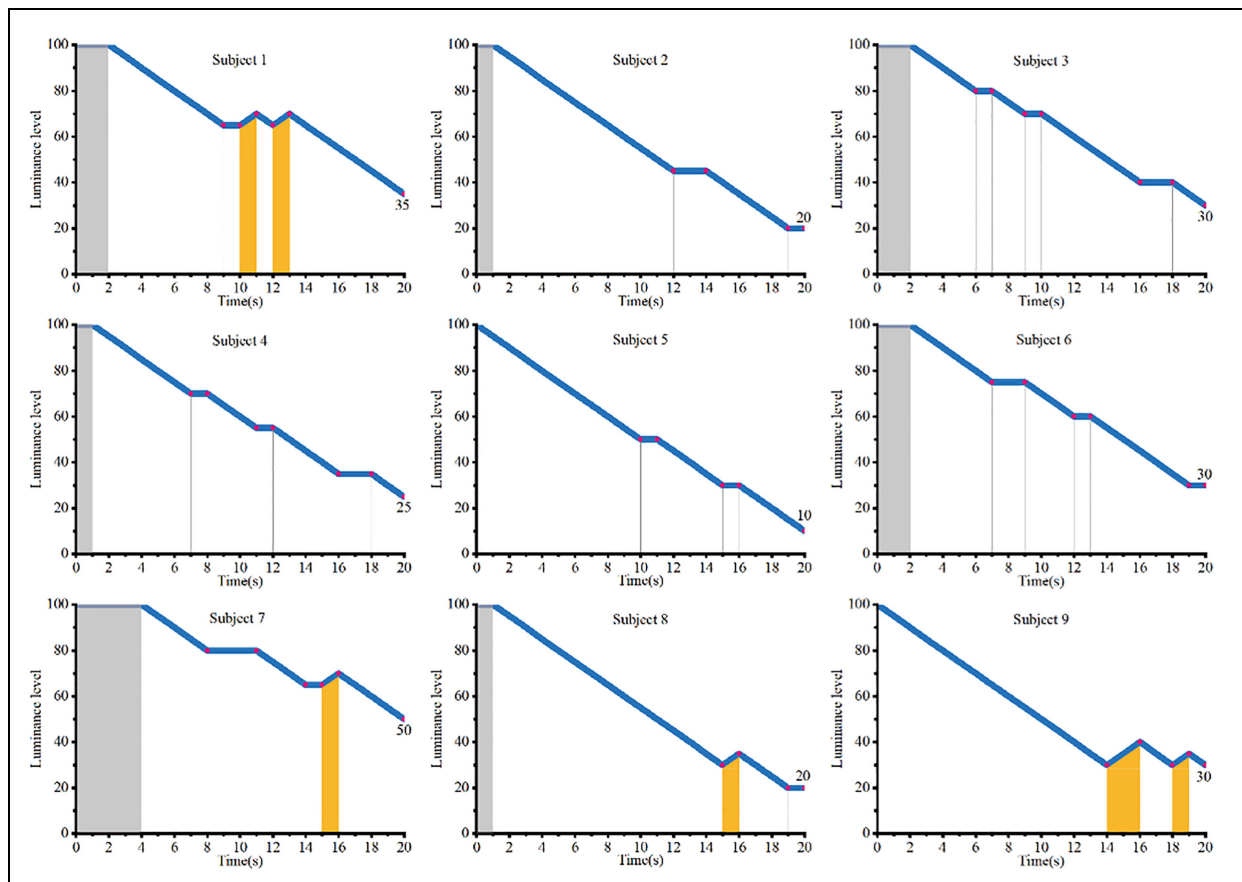
**Alternating brightness.** The luminance levels were set to 0 and the subjects were first asked to brighten the light

for 8 s, then hold for 14 s and finally dim the light for 8 s. The luminance change curve is shown in Figure 11.

Grey shading indicates the delay in the entry of the participants into the state, the magenta dots indicate abnormal time points and the light blue parts indicate the time when the light remains constant. The graph reveals that although certain participants could not enter and exit the hold state at 8 and 20 s, the results for all revealed a ‘trapezoid’ shape, which proved that the proposed lighting control scheme was feasible.

## Discussion

The use of BCI technology for real-time control of external intelligent devices has gradually become a new human-computer interaction solution. However, the accuracy of real-time recognition considerably affects the interaction experience and execution completion of the entire system. The traditional solution compensates for errors generated under real-time signals via the addition of EEG channels. Certain studies have also achieved accuracy improvements by improving feature recognition and classification algorithms. The proposed scheme focuses on diverting signals in the channel during real-time control, using only three channels to



**Figure 9.** Results of nine participants in the continuous darkening experiment.

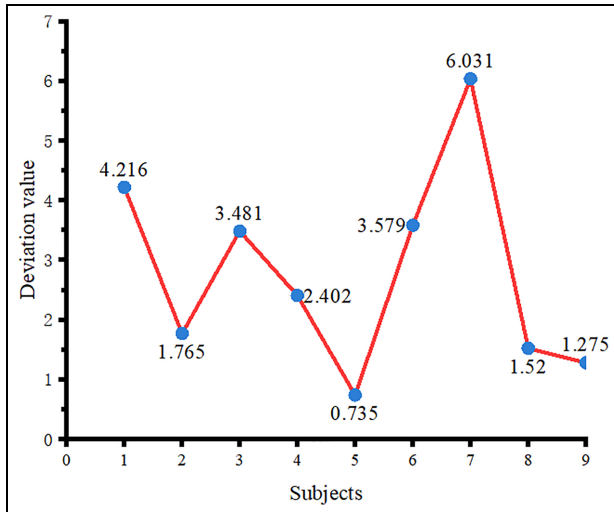


Figure 10. Dev value of continuous darkening experiment.

recognise MI EEG signal, thereby achieving high real-time three-class classification accuracy.

We compared the experimental results with those of previous studies, and the comparison results are presented in Table 2.

Table 2 reveals that the proposed real-time three-class classification outperformed of the methods proposed in other studies.

In the classification experiments, the recognition accuracy of the 'right' MI was higher than that of the 'left' MI. A possible reason for this phenomenon is that all nine participants were right-handed.

The three experimental results for each subject in the experiments with real-time control of LED correlate roughly positively with the categorical results in Table 1. A comparison of Figures 10 and 11 reveals that the number of participants who produced a delayed entry state, as well as the number of abnormal states, was considerably higher in the continuous darkening session than in the continuous brightening session. This phenomenon could be attributed to the fact that all nine participants were right-handed and therefore produced lower evoked potentials during the MI 'left'. In the alternation experiment, all nine participants could control the hold time at 11 s and above. However, Participants 1 and 6 both revealed varying degrees of fluctuation during the hold phase. One possible reason is the moods of these two participants fluctuated considerably when performing 'rest' tasks.

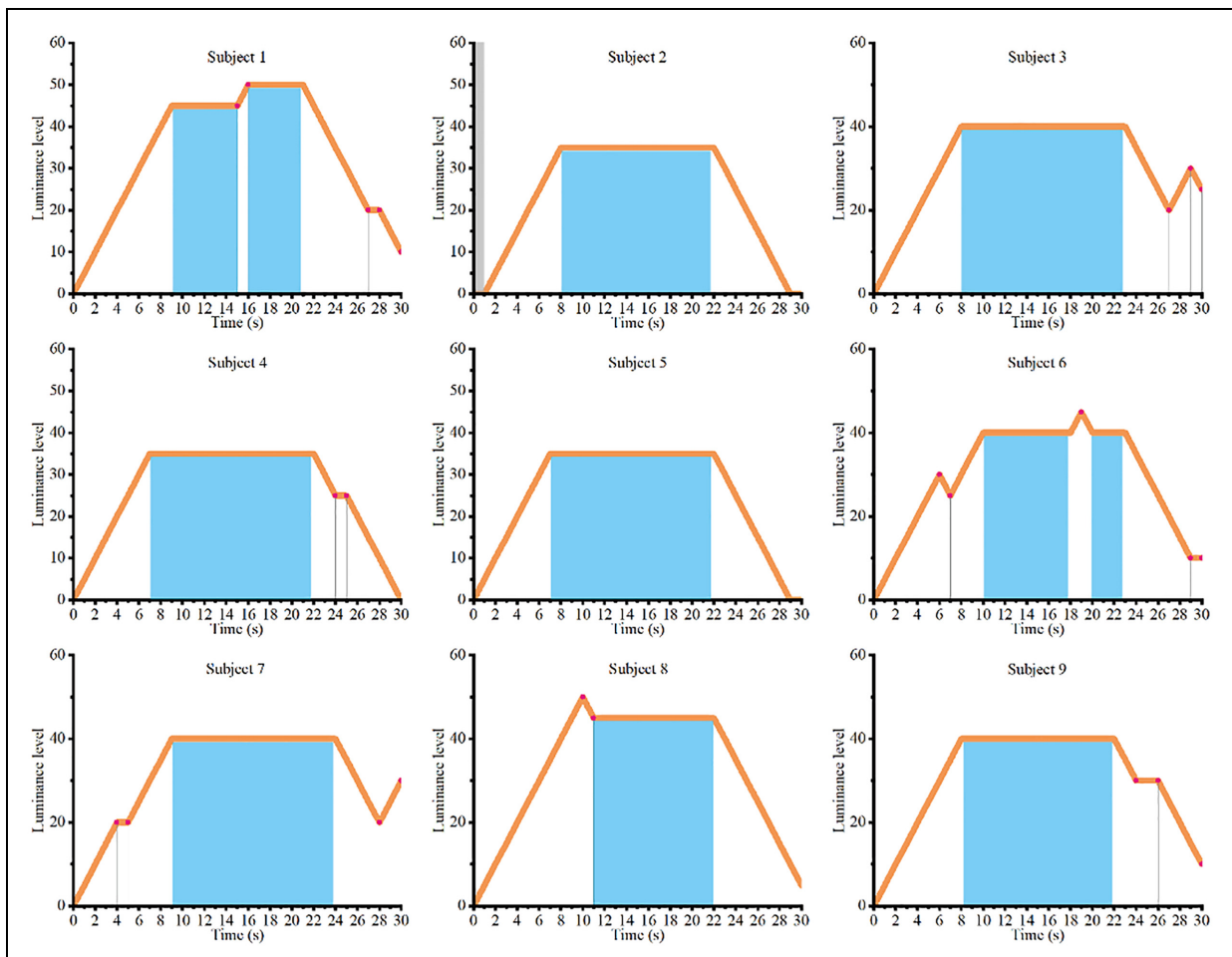


Figure 11. Results of nine participants in the alternation experiment.

**Table 2.** Comparison of classification accuracy of three-class-based motor imagery.

Groups	Classes state	Feature extraction	Classifier	Accuracy (%)
Ang et al. <sup>28</sup>	LH, RH, Feet	FB-CSP	MIRSR	63.7
Baziyad and Ridha <sup>29</sup>	LH, RH, Feet	Wavelet + CSP	SVM	75.5
Hasan and Gan <sup>30</sup>	LH, RH, Feet	CSP	LD-CRFs	74.1
Li et al. <sup>31</sup>	LH, RH, Feet	FB-CSP	Voting mechanism	68.6
Zhou et al. <sup>32</sup>	LH, RH, Feet	ICA spatial filters	SVM	86.9
Proposed	LH, RH, Rest	Channel selection FB-TRCSP	SVM (one vs rest)	90.3

There are still certain shortcomings in the study. Considering the length of time and the significance of the experimental effect, five luminance levels per second were set in the real-time control experiment. However, the system can divide the luminance into 140,000 levels, and the transmission interval can be as low as 4 ms. Thus, the fastest change in luminance was 250 levels per second, whereas approximately 560 s were required to complete 140,000 level changes. This process is not feasible in practice; thus, so the next step is to add acceleration control to the luminance adjustment based on the level of evoked potential to achieve fast and delicate control.

## Conclusions

We examined the real-time control of BCIs in intelligent devices. The experimental results indicated that the proposed label-based channel diversion preprocessing significantly improved the accuracy of real-time three-class classification (average real-time accuracy reaches 87.46%, with a maximum of 90.33%). In real environment lighting control experiments, the stability and reliability of the system have also been verified.

With the development of science and technology, as well as medical technology, BCI has attracted considerable research attention, and the proposed scheme effectively improves the accuracy of real-time three-class classification. Moreover, the improvement in accuracy achieved in this study is of considerable significance for the industrialisation of BCI.

## Author contributions

Jiakai Zhang: Methodology, Software, Validation, Writing – original draft, Visualisation. Boyang Xu: Software, Data curation, Methodology. Xiongjie Lou: Software, Validation, Formal analysis. Yan Wu: Funding acquisition, Resources. Xiaoyan Shen: Conceptualisation, Resources, Writing – review & editing, Supervision, Project administration, Funding acquisition.

## Declaration of conflicting interests

The author(s) declared no potential conflicts of interest with respect to the research, authorship, and/or publication of this article.

## Funding

The author(s) disclosed receipt of the following financial support for the research, authorship, and/or publication of this article: This work was supported by the National Natural Science Foundation of China under Grant [numbers 81371663 and 61534003]; the ‘Six talents peaks’ Project, China under Grant [number SWYY-116]; and the ‘226 Engineering’ Research Project of Nantong Government and the Postgraduate Research & Practice Innovation Program of Jiangsu Province, China under Grant [number KYCX21\_3085].

## References

- De Silva LC, Morikawa C and Petra IM. State of the art of smart homes. *Eng Appl Artif Intell* 2012; 25: 1313–1321.
- Qin LY, Nasir NM, Huq MS, et al. Smart home control for disabled using brain computer interface. *Int J Integr Eng* 2020; 12: 74–82.
- Xiong M, Hotter R, Nadin D, et al. A low-cost, semi-autonomous wheelchair controlled by motor imagery and jaw muscle activation. In: *2019 IEEE international conference on systems, man and cybernetics (SMC)*, Bari, Italy, 6–9 October 2019, pp.2180–2185. New York: IEEE.
- Yu Y, Liu Y, Jiang J, et al. An asynchronous control paradigm based on sequential motor imagery and its application in wheelchair navigation. *IEEE Trans Neural Syst Rehabil Eng* 2018; 26: 2367–2375.
- Xu B, Li W, Liu D, et al. Continuous hybrid BCI control for robotic arm using noninvasive electroencephalogram, computer vision, and eye tracking. *Mathematics* 2022; 10: 618–623.
- Borgheai SB, McLinden J, Zisk AH, et al. Enhancing communication for people in late-stage ALS using an fNIRS-based BCI system. *IEEE Trans Neural Syst Rehabil Eng* 2020; 28: 1198–1207.
- Peters B, Bedrick S, Dudy S, et al. SSVEP BCI and eye tracking use by individuals with late-stage ALS and visual impairments. *Front Hum Neurosci* 2020; 14: 595890.
- Pawuś D and Paszkiel S. BCI wheelchair control using expert system classifying EEG signals based on power spectrum estimation and nervous tics detection. *Appl Sci* 2022; 12(20): 10385.
- Abenna S, Nahid M, Bouyghf H, et al. EEG-based BCI: a novel improvement for EEG signals classification based on real-time preprocessing. *Comput Biol Med* 2022; 148: 105931.

10. Jeyabalan V, Samraj A and Kiong LC. Motor imagery signal classification using adaptive recursive bandpass filter and adaptive autoregressive models for brain machine interface designs. *Int J Bioeng Life Sci* 2007; 1(5): 242–249.
11. Qiu W, Fung KS, Chan FH, et al. Adaptive filtering of evoked potentials with radial-basis-function neural network prefilter. *IEEE Trans Biomed Eng* 2002; 49(3): 225–232.
12. Iacoviello D, Petracca A, Spezialetti M, et al. A real-time classification algorithm for EEG-based BCI driven by self-induced emotions. *Comput Methods Programs Biomed* 2015; 122(3): 293–303.
13. Lotze M and Halsband U. Motor imagery. *J Physiol Paris* 2006; 99: 386–395.
14. Pfurtscheller G. Functional brain imaging based on ERD/ERS. *Vision Res* 2001; 41: 1257–1260.
15. Khazi M, Kumar A and Vidya MJ. Analysis of EEG using 10: 20 electrode system. *Int J Innov Res Sci Eng Technol* 2012; 1: 185–191.
16. Feng QC. Design of brain-computer interface based on OpenBCI and OpenViBE. *Chin J Med Phys* 2020; 37: 210–219.
17. Thomas KP, Guan C, Lau CT, et al. A new discriminative common spatial pattern method for motor imagery brain-computer interfaces. *IEEE Trans Biomed Eng* 2009; 56: 2730–2733.
18. Wu XP, Zhou BY, Zhang L, et al. Recent progress and future development of spatial filtering technique in brain-computer interface. *J Anhui Univ Sci* 2017; 41: 14–31.
19. Talukdar U, Hazarika SM and Gan JQ. Adaptation of common spatial patterns based on mental fatigue for motor-imagery BCI. *Biomed Signal Process Control* 2020; 58: 101829.
20. Wu W, Chen Z, Gao X, et al. Probabilistic common spatial patterns for multichannel EEG analysis. *IEEE Trans Pattern Anal Mach Intell* 2015; 37: 639–653.
21. Wei Y, Wu Y and Tudor J. A real-time wearable emotion detection headband based on EEG measurement. *Sens Actuators A Phys* 2017; 263: 614–621.
22. Zahid SZ, Aqil M, Tufail M, et al. Online classification of multiple motor imagery tasks using filter bank based maximum-a-posteriori common spatial pattern filters. *IRBM* 2020; 41: 141–150.
23. Pisner DA and Schnyer DM. Support vector machine. In: Mechelli A and Vieira S (eds) *Machine learning: methods and applications to brain disorders*. London: Academic Press, 2020, pp.101–121.
24. Selim S, Tantawi MM, Shedeed HA, et al. A CSP\AM-BA-SVM approach for motor imagery BCI system. *IEEE Access* 2018; 6: 49192–49208.
25. Silva CR, de Araújo RS, Albuquerque G, et al. Interfacing brains to robotic devices-a VRPN communication application. In: Costa-Felix R, Machado J and Alverenga A (eds) *26th Brazilian congress on biomedical engineering, IFMBE proceedings*. Singapore: Springer, 2019, pp.597–603.
26. Zheng M, Yang B and Xie Y. EEG classification across sessions and across subjects through transfer learning in motor imagery-based brain-machine interface system. *Med Biol Eng Comput* 2020; 58: 1515–1528.
27. Chen H and Che L. Design and implementation for the PWM closed-loop feedback interface circuit of a sandwich capacitive accelerometer based on ARM. *Int J Mod Phys B* 2021; 35: 2150094.
28. Ang KK, Chin ZY, Wang C, et al. Filter bank common spatial pattern algorithm on BCI competition IV datasets 2a and 2b. *Front Neurosci* 2012; 6: 39.
29. Baziyad AG and Ridha D. A study and performance analysis of three paradigms of wavelet coefficients combinations in three-class motor imagery based BCI. In: *2014 5th international conference on intelligent systems, modeling and simulation*. Langkawi, Malaysia, 27–29 January 2014, pp.201–205. New York: IEEE.
30. Hasan BAS and Gan JQ. Conditional random fields as classifiers for three-class motor-imagery brain-computer interfaces. *J Neural Eng* 2011; 8: 025013.
31. Li B, Yang B, Guan C, et al. Three-class motor imagery classification based on FBCSP combined with voting mechanism. In: *2019 IEEE international conference on computational intelligence and virtual environments for measurement systems and applications (CIVEMSA)*, Tianjin, China, 14–16 June 2019, pp.1–4. New York: IEEE.
32. Zhou B, Wu X, Zhang L, et al. Robust spatial filters on three-class motor imagery EEG data using independent component analysis. *J Biosci Med* 2014; 2: 43–49.